Nondestructive damage detection scheme for steel bridges

Sherif Beskhyroun*, Shuichi Mikami**, and Toshiyuki Oshima***
シェリフ ベスキロウン*, 三上修一**, 大島俊之***

*Graduate Student, Dept. of Civil Eng., Kitami Institute of Technology, (165 Koen-cho, Kitami, 090-8507, Japan)
**Associate Professor, Dept. of Civil Eng., Kitami Institute of Technology, (165 Koen-cho, Kitami, 090-8507, Japan)
***Professor, Dept. of Civil Eng., Kitami Institute of Technology, (165 Koen-cho, Kitami, 090-8507, Japan)

This paper presents structural damage detection method based on changes in Transfer Function Estimate (TFE) for detecting damage, predicting its location and monitoring the growth in damage. This method assumes that the displacement or the acceleration response time histories at various locations along the structure both before and after damage are available for damage assessment. These responses are used to estimate TFE. The change of TFE between the baseline state and the current state is then used to identify the location of possible damage in the structure. The method is applied to the experimental and numerical data obtained from a railway steel bridge that is no longer in service. Several damage scenarios were introduced to the main girder of the test structure. Results show the method can be used to detect the damage, determine the exact location and measure the growth in damage with very good accuracy. The use of piezoelectric actuators as a local excitation source for large structures such as steel bridges is also presented. Experimental and numerical results show that the proposed approach may be successfully implemented on-line to detect the damage and to locate regions where damage occurred.
Key Words: Damage detection; Modal parameters; Health monitoring; Transfer Function

1. Introduction

There is a growing need for built-in monitoring systems for civil engineering infrastructures, due to problems such as increasing traffic loads and rising costs of maintenance and repair. In the past two decades, a significant amount of efforts have been directed towards the development of structural health monitoring (SHM) and non-destructive damage detection methods to manage civil structures more efficiently. Numerous papers are available in the technical literature related to non-destructive damage detection and evaluation, SHM, and instrumentation schemes. Significant efforts have also been focused on developing data collection procedures and damage detections schemes. The term SHM has gained wide acceptance in the past decade as a mean to monitor a structure and provide an early warning of an unsafe condition using real time data. The goal of SHM and other so called 'smart structures' technologies and concepts is to develop 'multifunctional' structures, i.e. structures which provide functionality in other areas besides the primary focus of carrying operational static, dynamic and fatigue loads, with the ultimate objective of providing an enhanced level of system performance. In addition to SHM, a broad range of smart technologies are under development at universities, sensor and actuator companies, and aerospace system manufactures. In recent years, there has also been a renewed interest in the damage diagnosis and health monitoring of existing highway bridges using vibration based damage identification techniques. Most vibration-based damage detection theories and practices are formulated based on the assumption that failure or deterioration would primarily affect the stiffness and therefore, affect the modal characteristics of the dynamic response of the structure[1-5]. If this kind of changes can be detected and classified, this measure can be further implemented for a bridge monitoring system to indicate the condition, or damage, or remaining capacity of the structures. It can also be used to evaluate the seismic behavior of the structures. However, conventionally defined modal parameters have been shown to be mildly sensitive in the detection of various types of bridge damages. Furthermore, the modal parameters of conventional modal testing such as frequencies and modal damping are global parameters, which cannot locate the damages[6]. Research efforts have been made to detect structural damage directly from dynamic response measurements in the time domain, e.g. the random decrement technique[7], or from frequency response functions (FRF)[8]. Also, some damage detection methods have been proposed to detect damage using system identification techniques[9,10]. In this paper, an algorithm based on changes in TFE is presented. The algorithm is used to detect damage, locate its position and monitor the increase in damage using only the measured data without the need for any modal identification or numerical models. The method is applied to the experimental and

numerical data extracted from a railway steel bridge after inducing some defects to its members. The damage was introduced to the bridge through the release of some bolts from some stiffeners located on the web of the main girder of the bridge. A future goal of a comprehensive bridge management system is to have a self-monitoring bridge where sensors feed measured responses (accelerations, strains, etc.) into a local computer. This computer would, in turn, apply a damage identification algorithm to this data to determine if the bridge has significantly deteriorated to the point where user safety maybe jeopardized. The local computer could then contact a central monitoring facility (via cellular phone) to notify the appropriate maintenance or safety officials of the bridge's current condition. If such a monitoring system is to be practical, it will have to identify the dynamic properties of the structure from ambient, traffic-induced vibration or using another controlled excitation technique. The ambient vibration has the advantage of being inexpensive and convenient since no equipment is needed to excite the structure. The service needs not be interrupted to use this technique. One difficulty with determining dynamic parameters of a structure undergoing ambient vibrations is that the forcing function is not precisely characterized. Modal testing has some weaknesses as well. One of these is the high level of noise, as compared to the signals. Another difficulty of using ambient vibration data to implement damage identification method presented in this study is to find two equal excitation forces (before and after damage), as required in this method. In this paper, the implementation of piezoelectric actuators[11-13] as a local excitation source for large structures such as steel bridges is presented. The advantages of using piezoelectric actuators instead of shakers, hammers or ambient vibrations will be discussed in details in the following chapters.

2. Theoretical description

A novel method is proposed herein for detecting damage, identifying its location and monitoring the increase in damage using TFE. This method assumes that the displacement or the acceleration response time histories at various locations along the structure both before and after damage are available for damage assessment. These responses are used to estimate TFE. The change of TFE between the baseline state and the current state is then used to identify the location of possible damage in the structure. The excitation forces used for the undamaged and damaged structure must have the same amplitude, location and waveform in order to ensure that the changes in TFE data are mainly due to damage. In order to overcome the problem of the limited number of identified modal parameters, TFE information estimated from the various accelerometer readings at all frequencies in the measurement range and not just the modal frequencies will be compared before and after damage using the proposed method. In order to identify the damage with more confidence, every measuring channel will be used once as a reference for other channels, which will create large sets of data. These sets of data can then be analyzed using statistical procedures to determine the damage location with more confidence, as will be explained in details in this section. Transfer functions are mathematical functions used to characterize the input-output relationships of linear systems, which can be described by the following relationship:

$$Y(f) = H(f) \times X(f) \tag{1}$$

or

$$H(f) = Y(f) / X(f) \tag{2}$$

where $H(f)$ is a transfer function, $Y(f)$ is the finite Fourier transform (FFT) of the measurement signal $y(t)$ and $X(f)$ is the FFT of the reference signal $x(t)$. In Eq. (1), it can be seen that $Y(f)$ will always be the input signal $X(f)$ multiplied by the transfer function $H(f)$, for every $X(f)$. We can imagine that the transfer function $H(f)$ is the object that is modifying the source signal $X(f)$. In this paper, the transfer function will be estimated between the structure's response at a measuring point $x(t)$ relative to a reference response $r(t)$ assuming that the response $x(t)$ represents the input force that is related to the response $r(t)$ by the transfer function. In this case, the transfer function represents a relation between the structure's responses at two different measuring points x and r.

Let $T_{xr}(f)$ denote the TFE which relates a response $x(t)$ to a reference response $r(t)$. Since every channel will be used as a reference for other channels, $T_{rx}(f)$ will represent the TFE which relates a response $r(t)$ to a reference response $x(t)$. The relative TFE between x and r can then be defined as:

$$R_{xr}(f) = T_{xr}(f) - T_{rx}(f). \tag{3}$$

$R_{xr}(f)$ represents the relative movement (response) between x and r in the frequency domain. If equal forces are used to excite the undamaged structure a number of times, then it is assumed that the same relative response, $R_{xr}(f)$, will be obtained each time. On the other hand, if damage occurs at (or near) the location of x or r (or both), then the value of $R_{xr}(f)$ will in turn change. The absolute difference in absolute value of $R_{xr}(f)$ before and after damage can then be defined as:

$$D_{xr}(f) = \left| |R_{xr}(f)| - |R^{*}_{xr}(f)| \right| \tag{4}$$

where the asterisk denotes the damaged structure. When the change in relative TFE, $D_{xr}(f)$, is measured at different frequencies on the measurement range from f_1 to f_m, a matrix $[\mathbf{D_r}]$ can be formulated as

$$\mathbf{D_r} = \begin{bmatrix} D_{1r}(f_1) & D_{1r}(f_2) & \cdots\cdots & D_{1r}(f_m) \\ D_{2r}(f_1) & D_{2r}(f_2) & \cdots\cdots & D_{2r}(f_m) \\ \cdot & \cdot & \cdots\cdots & \cdot \\ \cdot & \cdot & \cdots\cdots & \cdot \\ \cdot & \cdot & \cdots\cdots & \cdot \\ D_{nr}(f_1) & D_{nr}(f_2) & \cdots\cdots & D_{nr}(f_m) \end{bmatrix}_r \tag{5}$$

where n represents the number of measuring points and r represents the number of reference channel. In matrix $[\mathbf{D_r}]$, every column represents the changes in $D_{xr}(f)$ at different measuring channels but at the same frequency value. Each measuring channel will be used as a reference for the other channels ($r = 1 : n$). Therefore, the matrix $[\mathbf{D_r}]$ will be formulated n different times (3D matrix). The total change in the relative TFE in the frequency range of f_1 to f_m can be estimated from the sum of rows of matrix $[\mathbf{D_r}]$ as:

$$\mathbf{ST}_r = \begin{Bmatrix} \sum_f D_{1r}(f) \\ \sum_f D_{2r}(f) \\ \vdots \\ \sum_f D_{nr}(f) \end{Bmatrix}_r \quad (6)$$

where $f = f_1 : f_m$ and $r = 1 : n$.

The sum of the changes in the relative TFE over different frequencies using different references can be used as the indicator of damage occurrence. In other words, the first damage indicator is calculated from the sum of $\{\mathbf{ST}_r\}$ over different references as:

$$\mathbf{SST} = \sum_r ST_r \,. \quad (7)$$

This indicator is used to detect the occurrence of damage and monitor the growth in damage; however it was found to be a weak indicator of damage localization. A number of statistical decision making approaches will be employed to determine the location of damage. The first step in this procedure is the selection of the maximum change in relative TFE at each frequency line (the maximum value in each column of matrix $[\mathbf{D}_r]$) and discarding all other changes in relative TFE measured at other nodes. For example in matrix $[\mathbf{D}_r]$ (Eq. (5)), if $D_{3r}(f_1)$ is the maximum value in the first column then this value will be used as $M_{3r}(f_1)$ and other values in this column will be discarded. The same process is applied to the different columns in matrix $[\mathbf{D}_r]$ to formulate the matrix of maximum changes of relative TFE at different frequencies, $[\mathbf{M}_r]$. It should be noted that $[\mathbf{M}_r]$ is a 3D matrix where each value of r ($r = 1 : n$) formulates one matrix;

$$\mathbf{M}_r = \begin{bmatrix} 0 & 0 & 0 & .... & 0 \\ 0 & M_{2r}(f_2) & 0 & .... & 0 \\ M_{3r}(f_1) & 0 & 0 & .... & M_{3r}(f_m) \\ 0 & 0 & M_{4r}(f_3) & .... & 0 \\ . & . & . & .... & . \\ . & . & . & .... & . \\ 0 & 0 & 0 & .... & 0 \end{bmatrix}_r \quad (8)$$

In order to monitor the frequency of damage detection at any node, a new matrix $[\mathbf{L}_r]$ is formulated. The matrix consists of 0's at the undamaged locations and 1's at the damaged locations. At each frequency line (each column of $\mathbf{M}_r$), damage location will be represented by 1. For instance, in the matrix $[\mathbf{L}_r]$, a numerical value of 1 is inserted at the locations of $M_{3r}(f_1)$, $M_{2r}(f_2)$ ...etc, as follows:

$$\mathbf{L}_r = \begin{bmatrix} 0 & 0 & 0 & ..... & 0 \\ 0 & 1 & 0 & ..... & 0 \\ 1 & 0 & 0 & ..... & 1 \\ 0 & 0 & 1 & ..... & 0 \\ . & . & . & ..... & . \\ . & . & . & ..... & . \\ 0 & 0 & 0 & ..... & 0 \end{bmatrix}_r \,. \quad (9)$$

The summation of maximum changes in relative TFE is calculated from the sum of the rows of matrix $[\mathbf{M}_r]$ using different references. At each value of r, the sum of rows of matrix $[\mathbf{M}_r]$ will result in one vector. Therefore, n different vectors can be obtained;

$$\mathbf{SM}_r = \begin{Bmatrix} \sum_f M_{1r}(f) \\ \sum_f M_{2r}(f) \\ \vdots \\ \sum_f M_{nr}(f) \end{Bmatrix}_r \,. \quad (10)$$

In accordance with previous procedures, the total number of times of detecting the damage (number of frequency lines at which damage is detected) at different nodes is calculated from matrix $[\mathbf{L}_r]$ as:

$$\mathbf{SL}_r = \begin{Bmatrix} \sum_f L_{1r}(f) \\ \sum_f L_{2r}(f) \\ \vdots \\ \sum_f L_{nr}(f) \end{Bmatrix}_r \,. \quad (11)$$

At each value of r, $\{\mathbf{SL}\}$ represents the number of frequency lines at which damage is detected at each node. Assuming that the collection of the damage indices, $\{\mathbf{ST}_r\}$, $\{\mathbf{SM}_r\}$, and $\{\mathbf{SL}_r\}$, represents a sample population of a normally distributed random variable, normalized damage localization indicators are obtained as follows:

$$\mathbf{STN}_r = \frac{\{ST_r\} - \beta_{1r}}{\sigma_{1r}} \quad (12)$$

where β_{1r} and σ_{1r} represent the mean and standard deviation of the elements in vector $\{\mathbf{ST}_r\}$, respectively. It should be noted that for each value of r, new values of β_{1r} and σ_{1r} are estimated. Similarly, the normalized vectors $\{\mathbf{SMN}_r\}$ and $\{\mathbf{SLN}_r\}$ are formulated as:

$$\mathbf{SMN}_r = \frac{\{SM_r\} - \beta_{2r}}{\sigma_{2r}} \,, \quad (13)$$

$$\mathbf{SLN}_r = \frac{\{SL_r\} - \beta_{3r}}{\sigma_{3r}} \quad (14)$$

where β_{2r} and σ_{2r} represent respectively the mean and standard deviation of the elements in vector $\{\mathbf{SM}_r\}$ and β_{3r} and σ_{3r} represent respectively the mean and standard deviation of the elements in vector $\{\mathbf{SL}_r\}$. In order to reduce the effect of noise or measurement errors, a threshold level has to be defined. In vectors $\{\mathbf{STN}_r\}$, $\{\mathbf{SMN}_r\}$ and $\{\mathbf{SLN}_r\}$, values smaller than the threshold level will be discarded. In summary, damage localization indicators **SM** and **SL** are not normalized, no threshold is used and damage locations can be predicted at the maximum values or peaks. On the other hand, **STN**,

SMN and SLN are normalized and damage is predicted at the locations where their values exceed the threshold level. The advantages and drawbacks of each approach will be discussed.

3. Railway steel bridge: description and experimental setup

The experimental work in this research was performed on a railway steel bridge that is no longer in service. The bridge was removed from its service location several years ago and is now supported on two wooden blocks, as shown in Fig. 1. The bridge consists of two steel plate girders and two steel stringers support the train rails. Loads from the stringers are transferred to the plate girders by floor beams located at various intervals. The bridge dimensions and layout are shown in Fig. 2. The multi-layer piezoelectric actuator was used for local excitation. The actuator force amplitude was 200 N. Although this force amplitude seems to be very small compared to the shaker force or ambient vibration, it was enough to excite the web of the main girder at the position of the farthest accelerometer. Two actuators were used for exciting the web of the main girder in the horizontal direction. The actuators were located at the upper part on the web of the main girder (Fig. 2). The excitation forces used for the undamaged and damaged structure are random, equal in amplitude and have the same vibration waveform but the excitation force does not need to be measured. The main advantages of using piezoelectric actuators than using conventional excitation methods such as dynamic shakers, or ambient vibration can be summarized as follows:

- Actuator size is very small and can be handled easily. Therefore, it can be fixed to any structural element and remotely operated for continuous health monitoring of the structure.
- The traffic over the bridge does not need to be interrupted as the case of using dynamic shakers.
- Piezoelectric actuator can excite the structure at high frequencies, typically 1-900 Hz, thus activating the higher modes of the structure.
- Large numbers of vibration data can be recorded in a short time as the sampling rate in the case of using actuator can reach 2 kHz.
- The same excitation force (equal magnitude and the same waveform) can be produced for exciting both the undamaged and damaged structure, which is needed for applying damage identification technique studied in this paper.
- Undesired vibrations induced from wind, traffic or any other source can be avoided since the vibration data induced from the actuators can be generated at any desired time.

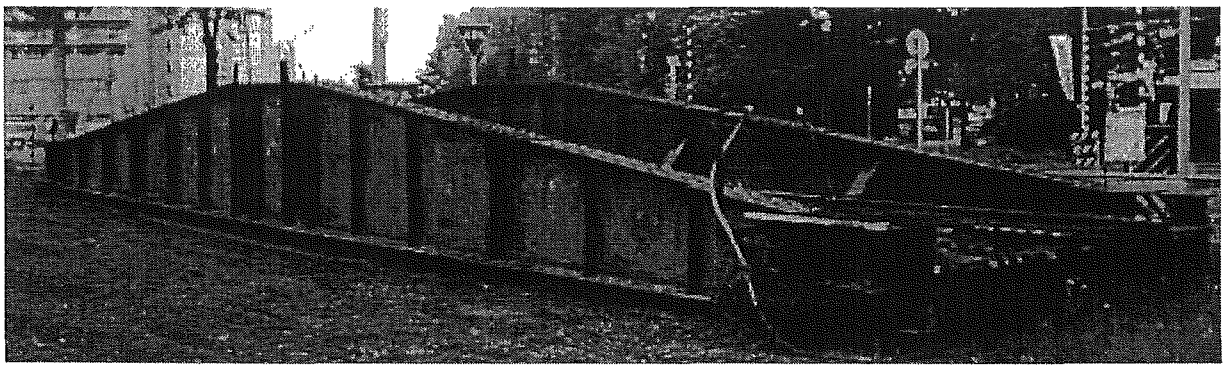

Fig. 1 Photo of the bridge

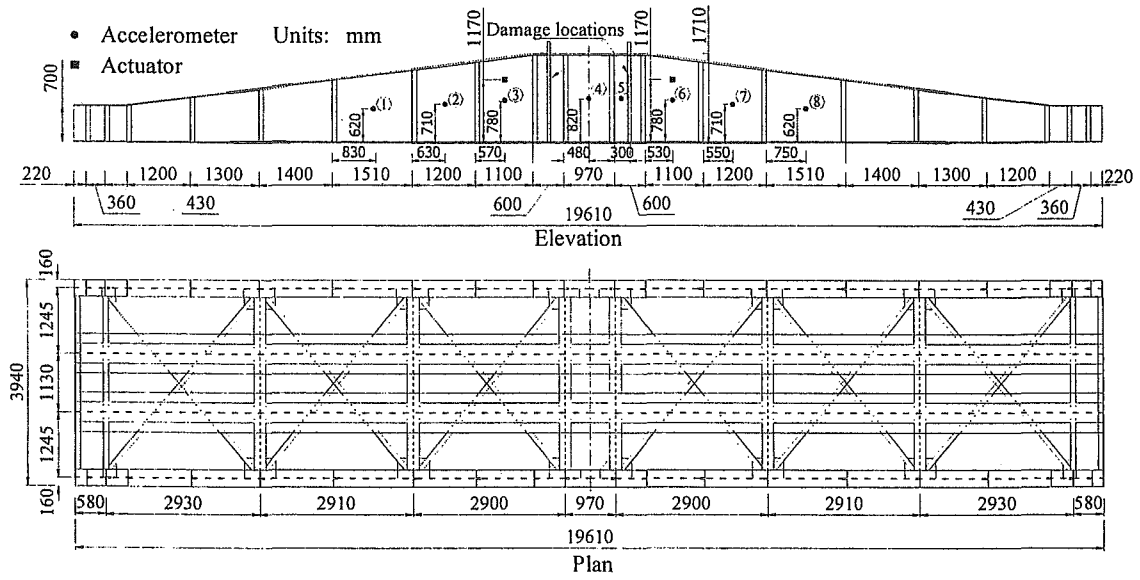

Fig. 2 Bridge layout and main dimensions

Eight accelerometers were used to measure the acceleration response in the horizontal direction. One accelerometer was mounted at the geometrical center of gravity of each panel of the main girder, as shown in Fig. 2. For this study, 20-second time histories were sampled at a rate of 1600 Hz, producing 32000 time points. A matrix of baseline undamaged data sets were recorded before damage was introduced to the structure. For each damage case, five separate time histories were recorded. All of the connections of different elements of the bridge are riveted and no damage could be introduced to these connections. Only two angles (look like stiffeners) are bolted to the web of main girder. Therefore, it was decided to remove the bolts one by one from the two stiffeners to introduce damage to the main girder.

4. Damage identification results

4.1 Removing one bolt near channel 5

The first level of damage was introduced to the bridge by removing the first bolt from the top of the right stiffener (near channel 5), as shown in Fig. 2. TFE is calculated at each measuring channel from the acceleration time history data using MATLAB Standard and MATLAB Signal Processing Toolbox[14, 15]. Hanning window of size 256 is applied to the time signals to minimize leakage. In this technique, the signal (acceleration data) is divided into overlapping sections (50% overlap) of the specified window length (256) and windows each section using the Hanning window function. In such case, the TFE can be measured at 129 frequency lines in the frequency range of 1-800 Hz (frequency step = 800*2/256). TFE at channel 5 using the response at channel 8 as a reference ($T_{5,8}$) and TFE at channel 8 using the response at channel 5 as a reference ($T_{8,5}$) for the undamaged structure are shown in Fig. 3 (a). The area between the two curves represents the relative TFE between channel 5 and 8 ($R_{5,8}$), as estimated from Eq. (3). The absolute values of $R_{5,8}$ are shown in Fig. 3 (b). Similarly for the damaged structure, $T^*_{5,8}$, $T^*_{8,5}$ are shown in Fig. 4 (a) and the absolute values of $R^*_{5,8}$ is shown in Fig. 4 (b). The change in the relative TFE at channel 5 due to the removal of one bolt from the stiffener near this channel can be observed by comparing Figs. 3 (b) and 4 (b). The absolute difference between these two figures (Eq. (4)) is shown in Fig. 5. In this figure, it is clearly indicated how the estimated change in $R_{5,8}$ depends on the frequency range. For example, the estimated changes in $R_{5,8}$ are relatively high in the frequency ranges of 50-100 Hz and 760-800 Hz compared to the changes at the frequency ranges of 0-50 Hz and 350-450 Hz. The frequency ranges that show higher changes in $R_{5,8}$ (better indication of damage) are randomly distributed in the total frequency range from 1-800 Hz. Therefore, it was decided to use TFE data in the total measurement range without the need to identify the best frequency range in which TFE has to be used in the proposed algorithm. The values of $D_{5,8}$ shown in Fig. 5 represent the 5th row in the 8th matrix $[\mathbf{D}_8]$ in Eq. (5). Every row in this matrix represents the changes estimated at one channel using channel 8 as a reference. Every new reference constructs a new matrix and thereby generates the 3d matrix $[\mathbf{D}_r]$. The following step is constructing the matrix of maximum changes $[\mathbf{M}_r]$ (Eq. (8)) and the corresponding matrix $[\mathbf{L}_r]$ (Eq. (9)) and

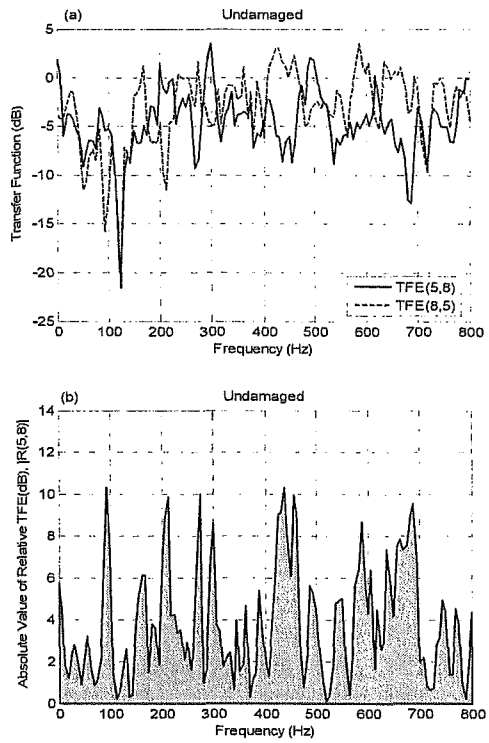

Fig. 3 TFE data and the associated relative TFE between channels 5 and 8 for undamaged structure

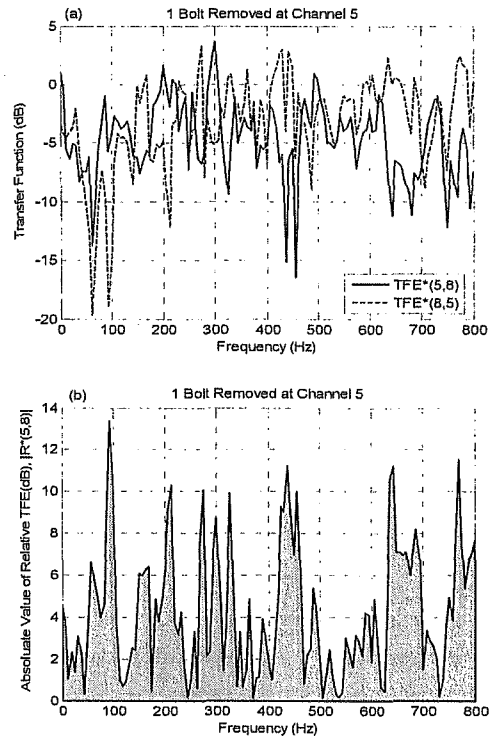

Fig. 4 TFE data and the associated relative TFE between channels 5 and 8 after removing 1 bolt near channel 5

then summing up the rows of each 2d matrix to estimate the damage indicators $\{\mathbf{SM}_r\}$ and $\{\mathbf{SL}_r\}$, respectively. Figs. 6 (a) and (b) show the resulting values of $\{\mathbf{SM}_r\}$ and $\{\mathbf{SL}_r\}$, respectively. At each reference

number, the estimated values in each vector are drawn using waterfall curves. Although the values at the measuring channels are discrete, it was decided to use continuous line to connect them instead of using bars in order to enhance the visualization of the results. In Fig. 6 (a), the maximum reading is indicated accurately at channel 5 using various reference channels (except channel 5). However, the accuracy of detecting the damage at channel 5 depends slightly on the used reference. It should be noted that when one channel is used as a reference, it cannot be used to detect the damage at its location at the same time. For example, the reading at channel 7 at the reference number 7 equal 0. This is simply because $R_{xx} = R^*_{xx} = 0$ (Eq. (3)) and hence $D_{xx} = 0$ (Eq. (4)). Therefore, when the channel near the damage location is used as a reference, it will always produce false positive readings at other channels. Thus, damage at one location can be predicted using at most (n-1) references. $\{\mathbf{SL}_r\}$ is used to estimate the total number of frequency lines at which damage is detected. In this study, the total frequency range from 1-800 Hz is divided to 129 lines (see Fig. 5). As indicated in Fig. 6 (b), damage at channel 5 is detected at about 50 frequency lines out of 129 lines that were used to estimate TFE data. This index is useful for indicating the confidence of detecting damage at a certain location. In Figs. 6 (a) and (b), although the maximum reading exists at channel 5 using various references, the readings at the undamaged locations sometimes degrade the accuracy of locating damage. It was, therefore, decided to create new damage localization indicators that can locate the damage more accurately. The proposed damage localization indicators presented in Eqs. (12-14) are normalized to allow for better comparison. Furthermore, a threshold level is defined to eliminate the readings at the undamaged locations that usually results from the presence of noise or measurement errors. In this study, the threshold level equals one. The values of $\{\mathbf{STN}_r\}$, $\{\mathbf{SMN}_r\}$ and $\{\mathbf{SLN}_r\}$ indices below the threshold level are related to undamaged cases and the values above (or equal to) the threshold level identify a potentially damaged element. The main task is then selecting an adequate threshold level in order to define the real damaged elements. This threshold level can be considered as a discriminating level. If this acceptance criterion is placed at a too high level (threshold = 1.5), some damages will be unrevealed. At a proper level (threshold = 1), clear discrimination will result. If the acceptance criterion is too low (threshold = 0.5), several false alarms will result. Therefore, an adequate level must be determined allowing clear discrimination. In this study, using a threshold level equal 1.0 for the test structure and its FEM has yielded the most accurate results. However, the best threshold level for a different structure in different circumstances may differ depending on many factors such as the type of the structure, level of noise, experimental variations, environmental changes, damage location and damage size. In order to generalize the threshold level approach based on the proposed method, the effect of these factors on more sophisticated structures needs to be studied. Using an accurate FEM of the structure to investigate several scenarios of damage, the effect of noise and the effect of environmental changes can be a useful tool to determine a good threshold level. The resulting values of $\{\mathbf{STN}_r\}$, $\{\mathbf{SMN}_r\}$ and $\{\mathbf{SLN}_r\}$ for this case of damage are shown in Figs. 6 (c), (d) and (e), respectively. Damage is located very accurately at channel 5 without any false positive readings at every reference channel except the reference number 7, using damage indicator **STN**. Damage indicator **SMN** shows better results where the damage is located

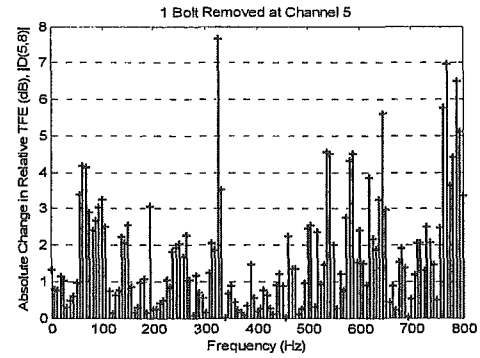

Fig. 5 The absolute difference in the relative TFE between channels 5 and 8 after removing 1 bolt near channel 5

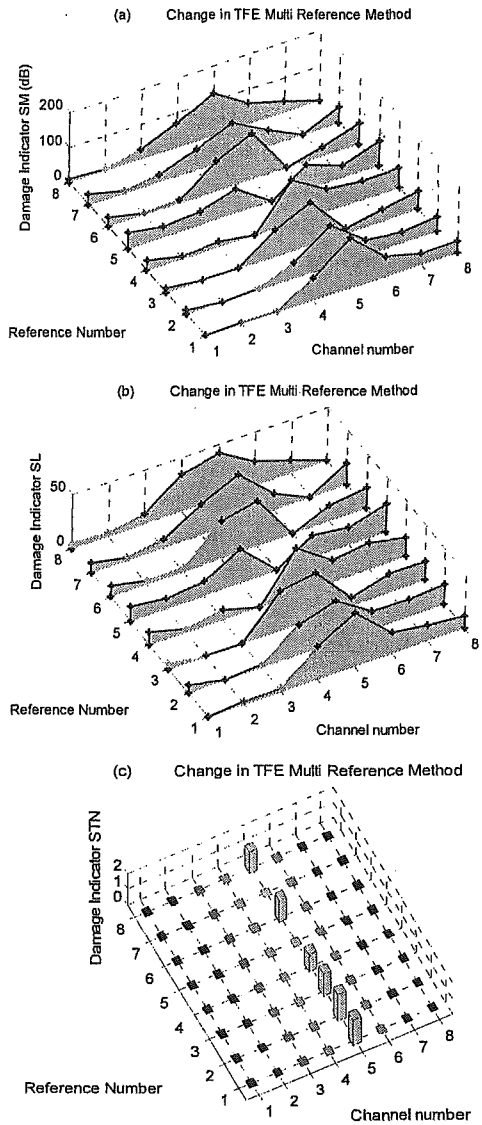

Fig. 6 Damage identification results after removing 1 bolt near channel 5

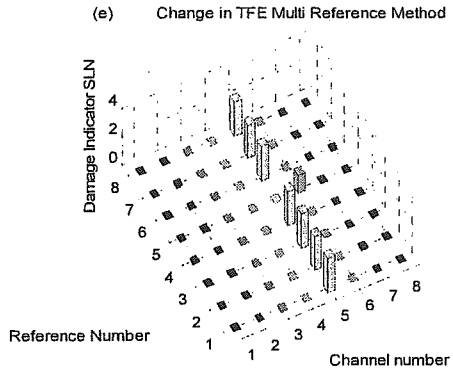

Fig. 7 (Cont.) Damage identification results after removing 2 bolts near channel 5

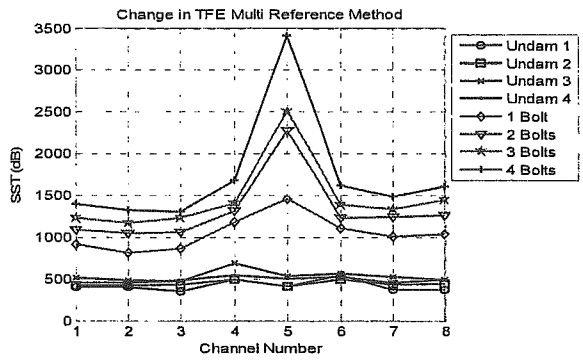

Fig. 8 Monitoring the growth in damage near channel 5

measurement errors, environmental or operational loads from the changes attributed with damage. Because of this need, the experiment was performed five times on the undamaged structure prior to the introduction of any damage. Four different combinations of TFE data obtained from the undamaged structure are used to estimate the values of **SST**. For example, the fourth set of data is used to estimate R in Eq. (4) and the first set of data is used to estimate R^*, then the resulting values of **SST** are plotted in Fig. 8 as indicated by the legend Undam 1. Similarly, the remaining sets Undam 2, Undam 3 and Undam 4 are estimated and plotted in the same figure. The values of **SST** was determined using TFE data in the frequency range of 1–800 Hz. The total change in TFE ranged from about 400 to 600 dB. The estimated changes in TFE are obviously due to the presence of noise and measurement errors. The upper limit of this range can be used as a threshold for the damage indicator **SST**. It is then assumed that if **SST** exceeds the threshold limit, this will indicate the occurrence of damage. In this study, the estimated threshold is based only on changes due to noise or measurement errors. However, in order to determine a more practical threshold, more data are needed to account for the changes in TFE caused by changes in temperature over different seasons or from operational loads. When the first level of damage was introduced to the bridge, the values of **SST** increased at most of channels to around 1000 dB and increased at the damage location to around 1500 dB, exceeding the threshold limit at all channels. The increase in **SST** at the undamaged locations is due to the fact that damage at one location changes the response, and hence TFE data, significantly at the close sensors locations and slightly at the more far sensors.

Since a serious damage to a structure is usually the result of the growth of less serious damage, it is important to have the ability to measure the growth in damage. We need to be able to monitor this growth for the purpose of bridge maintenance. The resulting damage indicator values of the damage indicator **SST** for four levels of actual damage – removing one to four bolts are shown Fig. 8 and indicated by the legends 1 Bolt through 4 Bolts, respectively. It is clearly indicated in this figure how the values of **SST** increase with increase in the damage level. Unfortunately, the damage severity cannot be identified quantitatively. However, for the same damage locations but different levels of damage compared with Fig. 8, the amplitude levels are higher for the cases of more severe damage, which can represent the damage severity to some extent.

4.4 Multiple damage

Most studies concerning crack detection deal with a single crack. The case of multiple cracks has not received the same degree of attention. The problem of detection of location of a number of faults in a component simultaneously is much more involved and complex than the case of a single crack. In the present damage case, equal amounts of damage were introduced to the two stiffeners located on the web of the main girder (Fig. 2). Channel 5 is located 15 cm from the centerline of the first damaged stiffener while channel 3, the nearest sensor to the second damage location, is located 53 cm from the centerline of the second damaged stiffener. As explained previously, the maximum change at each frequency line will be selected (the maximum value in each column in Eq. (5)) which indicates damage at this node. Therefore, damage is usually detected at only one location at each frequency line unless the same maximum value exists at more than one node which rarely occurs. However, the maximum change at another frequency line may indicate the damage at the second location. Moreover, using multiple reference channels can be useful in this case; as one reference may give accurate results in detecting the damage at one location while another reference may detect the damage at the second location. This underlines the importance of using all the frequency lines in the total measurement range as well as using each measuring channel as a reference. The first level of damage is introduced by removing one bolt from the top of each stiffener. The predicted results using different damage indicators are shown in Fig. 9. Damage indicators **SM** and **SL** show the predicted results without normalizing the data or using threshold as in case of using **STN**, **SMN** and **SLN**. It is clearly indicated in Fig. 9 how the selection of the reference channel affects on the results. In case of using damage indicators **STN**, **SMN** and **SLN**, damage indicator **SLN** showed the most accurate results while **STN** showed the least accurate one. The growth in damage could also be monitored accurately using damage indicator **SST**, as shown in Fig. 10. The damage level gradually increased at the two locations by removing more bolts from the two stiffeners. **SST** values at channel 5 are higher than its values at channel 3 for most of the damage levels because channel 5 is closer to the damage location.

accurately using all the references. Damage indicator **SLN** has shown the least accurate results and some false positive readings appeared at channel 4 at references number 3, 6 and 8. If damage location is predicted at one channel using all the references (except the same channel), then the identified damage locations using this channel as a reference should be ignored.

4.2 Removing two bolts near channel 5

The amount of damage increased in this case by removing one more bolt from the top of the right stiffener (Fig. 2). Damage identification results are shown in Fig. 7. Similar results are obtained in this case compared to the results of the previous case (removing one bolt) and can be summarized as follows:

- Damage indicator **SM** indicated the damage location at channel 5 more clearly than the previous case of damage as the indicator values at channel 5 increased and the values at the undamaged locations decreased.
- The number of frequency lines at which damage is detected accurately at channel 5 increased significantly in this case as determined by the damage indicator **SL**. Damage is detected at the correct location at approximately 100 frequency lines out of 129 frequency lines (Fig. 7 (b)), achieving one of the most important objectives of any damage identification algorithms which is to ascertain with confidence if damage is present or not.
- Normalized damage indicator **STN**, **SMN** and **SLN** identified damage location at channel 5 using all the references without any false positive readings (Figs. 7 (c), (d), and (e)).
- Damage location is identified accurately using various damage indicators regardless of the location of the reference channel.

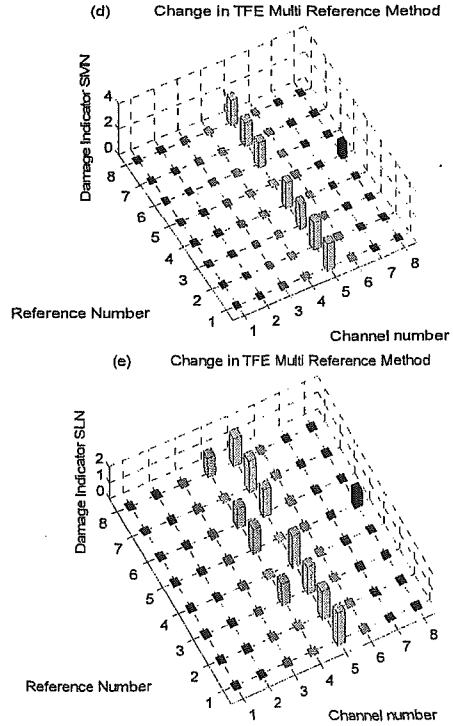

Fig. 6 (Cont.) Damage identification results after removing 1 bolt near channel 5

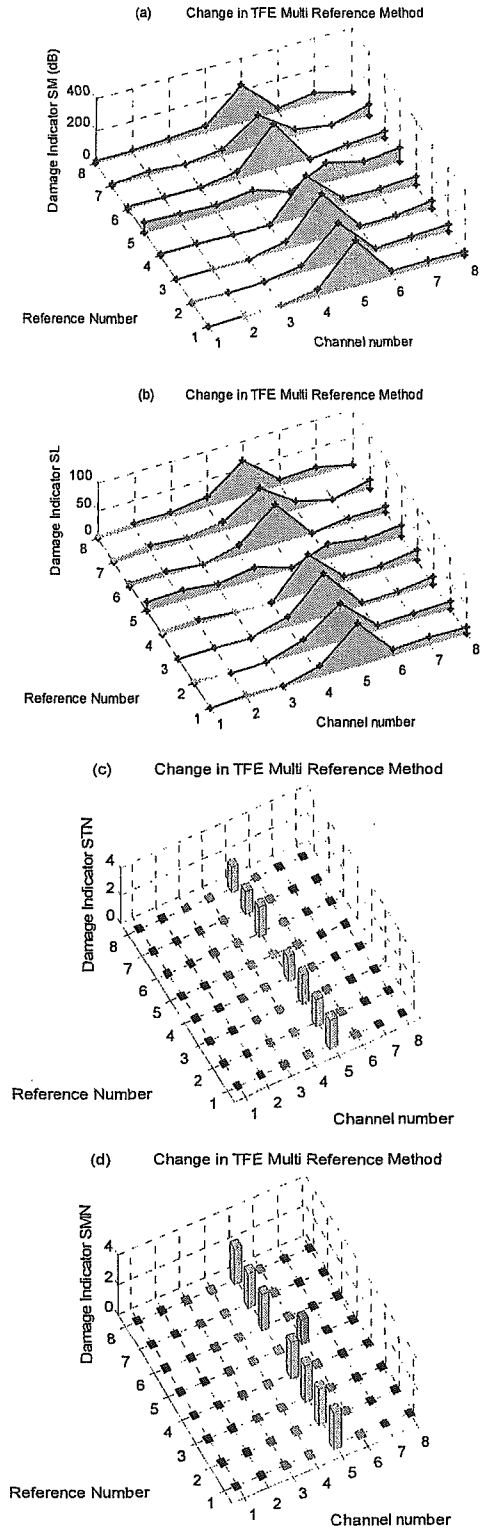

Fig. 7 Damage identification results after removing 2 bolts near channel 5

4.3 Monitoring the growth in damage at channel 5

As discussed previously, damage indicator **SST** (Eq. (7)) will be used to detect the occurrence of damage and monitor the increase in damage. Therefore, it is important to define a threshold of the total change in TFE that classifies the changes in TFE due to noise,

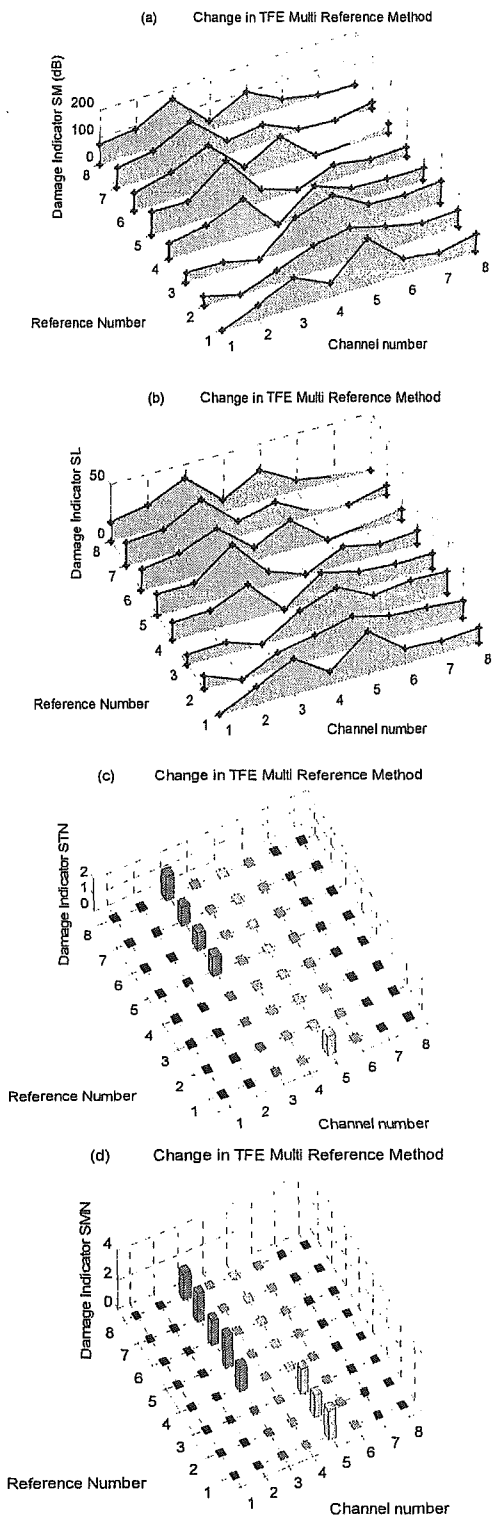

Fig. 9 Damage identification results after removing 1 bolt near channels 3 and 5

5. Numerical data

The finite element model of the bridge is created using Structural Analysis Program, SAP2000[16]. Main girders and cross beams are simulated by shell elements (Fig. 11). The FE model contains 1878

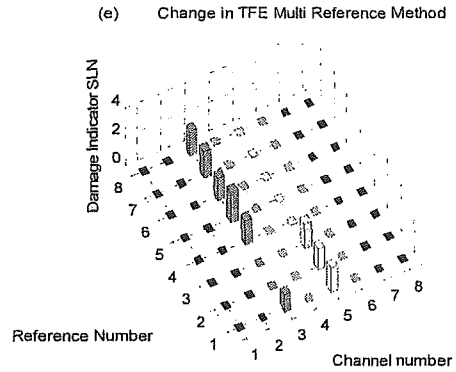

Fig. 9 (Cont.) Damage identification results after removing 1 bolt near channels 3 and 5

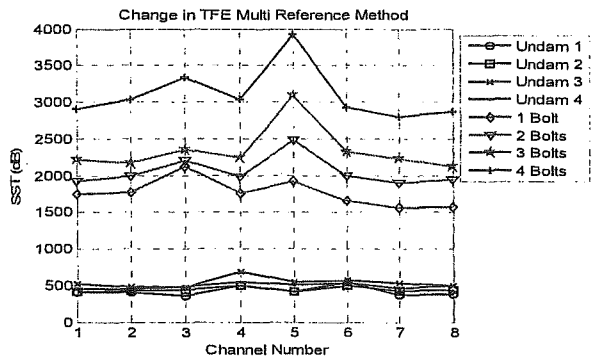

Fig. 10 Monitoring the growth in damage near channels 3 and 5

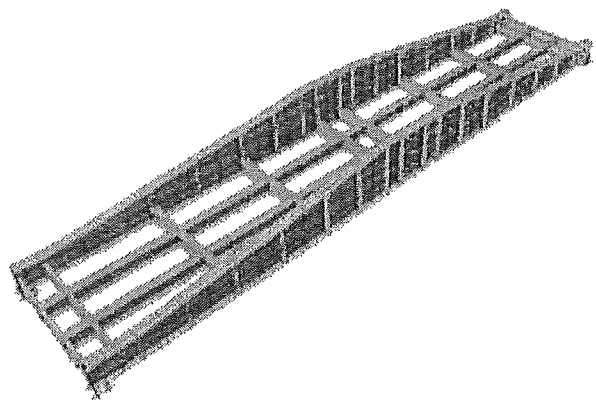

Fig. 11 Numerical model of the bridge

shell elements and 10508 active degrees of freedom. The weight density of steel is assumed to be 77 kN/m^3 and the modulus of elasticity of steel is assumed to be 206 GPa. Acceleration response in the horizontal direction is measured at eight nodes (N1-N8), as shown in Fig. 12. 20-second time histories were collected at 0.000625 second increments, producing 32000 time points to simulate the experimental data. The main objective of using the numerical data is to assess different effects rather than noise or measurement errors on the accuracy of the obtained results from the studied damage identification method. Moreover, the numerical model can be used to evaluate the performance of the damage identification method to detect different

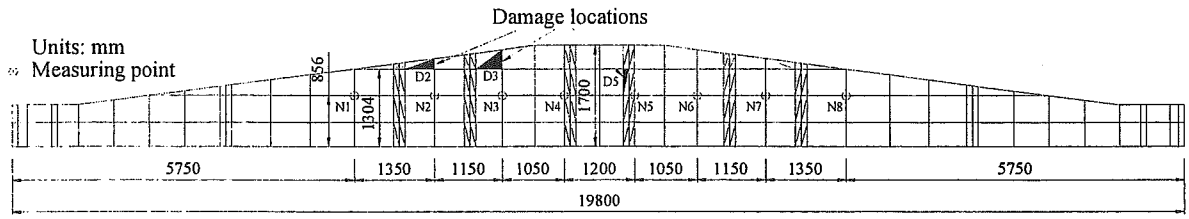

Fig. 12 The location of measuring points and damaged areas in the numerical model

types of damage at different locations. Three cases of damage are introduced to the numerical model by reducing the thickness of one shell element by 10% (1.1 mm). Damaged locations are indicated by the shadowed areas D2, D3 and D5 (Fig. 12). Mode shapes in the frequency range of 1-140 Hz could be identified using SAP2000. TFE in this frequency range is estimated using the same window size of 256 and the same sampling rate of 1600, producing 22 frequency lines. The predicted results using damage indicators **SL** and **SLN** for the three damage locations D2, D3 and D5 are shown in Figs. 13, 14 and 15, respectively. For damage locations D2 and D3, damage is detected at the nearest measuring point at about 20 frequency lines out of 22 lines using all the references. On the other hand, damage location D5 is detected at less frequency lines and some false positive readings are predicted (using **SL** only) though the numerical data does not contain any noise or measurement errors. The main reason involved here is that at each frequency line, the dynamic response at different measuring locations represents one operational mode shape. If this mode contains a node (i.e. zero amplitude) at the damage location, this may reduce the chance of predicting damage at this location and hence produce a false positive reading. It is, again, recommended that TFE be used in the total measurement range to reduce the effect of undesired frequency lines.

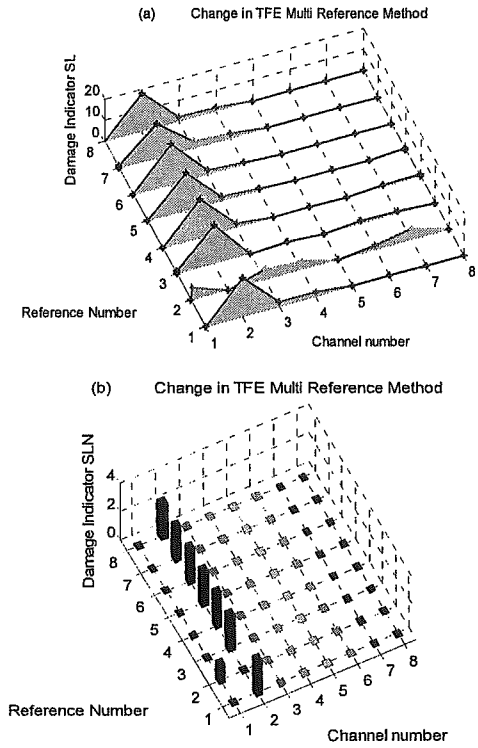

Fig. 13 Damage identification results for damage location D2 using numerical data

6. Comparing the proposed method with a previously reported method

In this section, the proposed method will be compared to a previously reported method[17] by the author. The previous method is based on changes in Power Spectral Density (PSD) caused by damage. For more details about this method, the reader is referred to the cited reference. The main differences between the two methods can be summarized as follows:

- The previous method estimates PSD magnitudes from the acceleration data at different measuring channels. Then use the changes in PSD magnitude to identify damage. The proposed method uses the relative TFE between two measuring points to identify damage.
- Different statistical procedures are used in the two methods to identify the damage.
- PSD method shows damage identification results at each measuring channel using various damage localization indicators. The proposed method shows damage identification results at each channel versus the reference channel that is used to calculate TFE data.

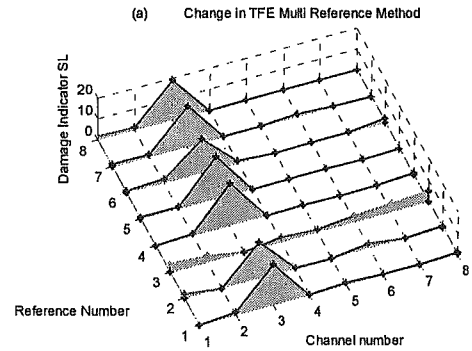

Fig. 14 Damage identification results for damage location D3 using numerical data

The two methods are similar in the following respects:

- Both methods use the structure's response without the need to measure the excitation force.
- Both methods can use the structure response in the frequency domain in the total measured frequency range.

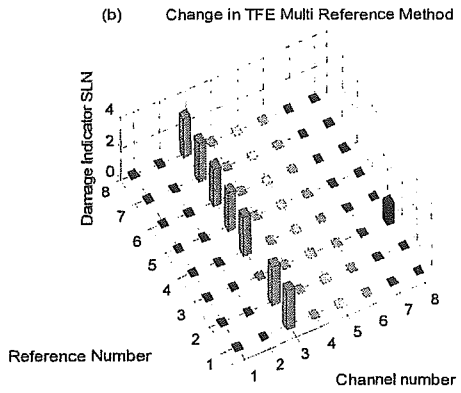

Fig. 14 (Cont.) Damage identification results for damage location D3 using numerical data

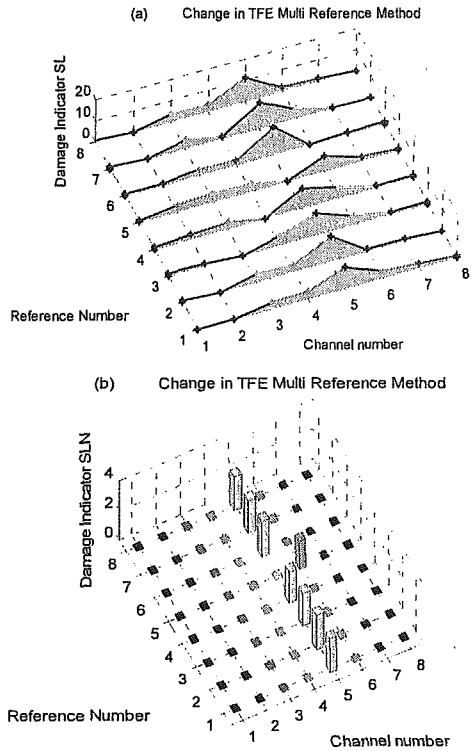

Fig. 15 Damage identification results for damage location D5 using numerical data

Fig. 16 shows PSD method results after removing one bolt from the stiffener near channel 5 using damage localization indicator 1. The false positive reading at channel 8 may degrade the accuracy of identifying damage location. The same remark is also observed for the case of double damage after removing one bolt from two stiffeners near channels 3 and 5, as shown in Fig. 17. When PSD is applied after removing two bolts from the stiffeners near channels 3 and 5, the predicted results at channel 5 is much bigger than that at channel 3 which reduce the confidence of predicting damage at this location (Fig. 18). The corresponding results of this case using damage localization indicator SMN are shown in Fig. 19. The previous drawbacks of PSD method are avoided in the proposed method by showing the results at

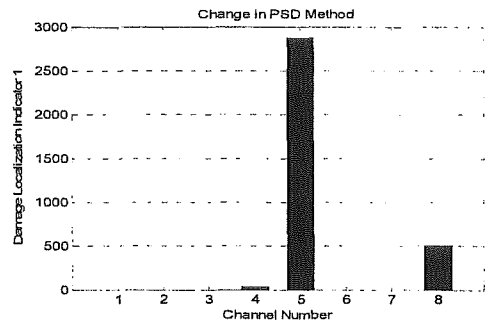

Fig. 16 Damage identification results after removing 1 bolt near channel 5 using PSD method

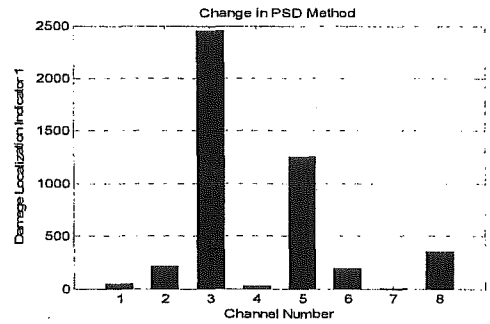

Fig. 17 Damage identification results after removing 1 bolt near channels 3 and 5 using PSD method

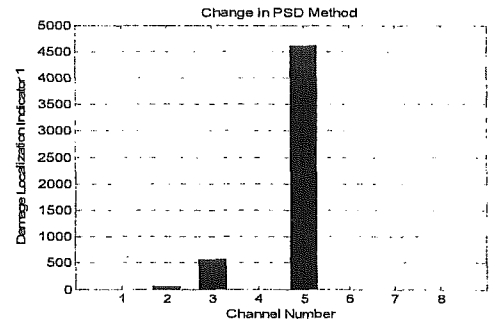

Fig. 18 Damage identification results after removing 2 bolts near channels 3 and 5 using PSD method

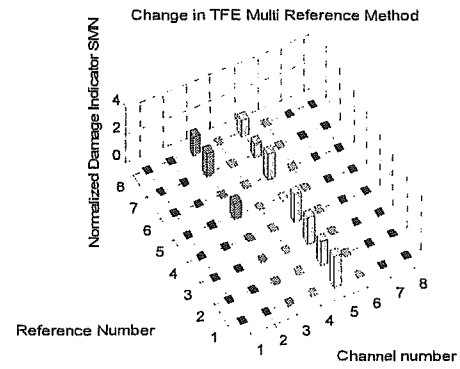

Fig. 19 Damage identification results after removing 2 bolts near channels 3 and 5 using the proposed method

each location versus the reference channel that is used to estimate the TFE data. In this case, the predicted damage location may be detected (n-1) times which increase the confidence of detecting damage at various locations.

7. Conclusions

This paper presents a novelty detection technique for structural damage diagnosis, using TFE data. TFE is calculated from the acceleration response at every channel relative to a reference channel and every channel is used as a reference to other channels to create a large number of information. Moreover, TFE magnitude at each frequency value is used in the proposed method. This accumulated information is then used for statistical procedures to identify the damage location with high confidence. The proposed method encompasses the first three steps of the process of damage detection – existence, localization and monitoring the growth in damage based only on the measured data without the need for any modal identification or numerical models. The technique presented here may allow some progress in in-service monitoring of steel bridges where the acceleration data can be transferred via wireless methods and the piezoelectric actuators can be used for local excitation. The proposed approach is demonstrated using experimental and numerical data obtained from a railway steel bridge. The new method shows very high accuracy in predicting damage location and monitoring growth in damage. The high detection performance, combined with the simple computation structure and the easy implementation could lead to a promising real-time damage detection system.

Acknowledgement

This research is supported by the Grant-in-Aids for Scientific Research, Ministry of Education. The authors wish to express their gratitude for this support. Special thanks are owed to Dr. Yamazaki, Mr. Tsubota and Mr. Okuyama (Kitami Institute of Technology) for the preparation of the experimental setup.

References

1) Doebling S. W., C. R. Farrar, M. B. Prime, and D. W. Shevitz, *Damage Identification and Health Monitoring of Structural and Mechanical Systems from Changes in their Vibration Characteristics*, A Literature Review, Los Alamos National Laboratory Report, LA-13070- MS, 1996.
2) Farrar C. R. et al., *Dynamic Characterization and Damage Detection in the I-40 Bridge Over the Rio Grande*, A Literature Review, Los Alamos National Laboratory Report, LA-12767- MS, 1994.
3) Farrar C. R. and D. A. Jauregui, *Damage Detection Algorithms Applied to Experimental and Numerical Model Data from the I-40 Bridge*, Los Alamos National Laboratory Report, LA-12979-MS, 1996.
4) Sampaio R. P. C., Maia N. M. M. and Silva J. M. M., Damage detection using the frequency-response-function curvature method, *Journal of Sound and Vibration*, 226(5), pp. 1029-1042, 1999.
5) Peeters B., Maeck J. and De Roeck G., Vibration-based damage detection in civil engineering: excitation sources and temperature effects, *Smart Materials and Structures*, 10, pp.518-527, 2001.
6) S.T. Xue, N. Fujitani, Z.B. Wei and H.S. Tang, Comparison of variations of natural frequencies for wooden structural models with and without damages part 2, shaking table based results, *Proceedings of the international conference on Structural Health Monitoring and Intelligent Infrastructure*, China, pp 1101-1104, 2006.
7) J. C. S. Yang, J. Chen and N. G. Dagalakis, Damage detection in offshore structures by the random decrement technique, *Journal of Energy Resources Technology*, American Society of Mechanical Engineers 106, 38-42, 1984.
8) R. G. Flesch and K. Kernichler, Bridge inspection by dynamic tests and calculations dynamic investigations of Lavent bridge, *workshop on Structural Safety Evaluation Based on System Identification Approaches* (H. G. Natke and J. T. P. Yao, editors), 433-459, Lambrecht/ Pfalz, Germany: Vieweg & Sons, 1988.
9) S. F. Masri, R. K. Miller, A. F. Saud and T. K. Caughey, Identification of nonlinear vibrating structures, *Journal of Applied Mechanics 54*, 923-929: Part I-formulation, 1987.
10) H. G. Natke and J. T. P. Yao, System identification methods for fault detection and diagnosis, *International Conference on Structural Safety and Reliability*, American Society of Civil Engineers, New York, 1387-1393, 1990,
11) Oshima T., Yamazaki T., Onishi K. and Mikami S., Study on damage evaluation of joint in steel member by using local vibration excitation, (In Japanese), *Journal of Applied Mechanics JSCE*, Vol.5, pp.837-846, 2002.
12) Beskhyroun S., Oshima T., Mikami S., Yamazaki T., Damage detection and localization on structural connections using vibration based damage identification methods, *Journal of Applied Mechanics, JSCE*, Vol.6, pp. 1055-1064, 2003.
13) Beskhyroun S., Mikami S., Oshima T. and Yamazaki T., Modified damage identification algorithm based on vibration measurements, *Journal of Applied Mechanics, JSCE*, Vol.7, pp. 97-107, 2004.
14) MATLAB *Reference Guide*, The Math Works, Inc., Natick, MA, 2003.
15) MATLAB *User's Guide*, The Math Works, Inc., Natick, MA, 2003.
16) SAP2000, *Integrated Finite Element and Design of Structures*, Analysis Reference Manual, Computers and Structures, Inc. Berkeley, CA, USA, 1995.
17) Beskhyroun S., Mikami S., Oshima T. and Tsubota Y., Structural damage identification algorithm based on changes in power spectral density, *Journal of Applied Mechanics, JSCE*, Vol.8, pp. 73-84, 2005.

(Received: April 13, 2006)